ACS Partner Journal

ENVIRONMENT & HEALTH

Open Access

pubs.acs.org/EnvHealth

Article

Theoretical Investigation of Cytochrome P450 Enzyme-Mediated Biotransformation Mechanism of BHPF: Unveiling the Metabolic Safety Aspects of an Alternative to BPA

Wenxiao Pan, Shuming He, Yinzheng Yang, Yongdie Yang, Qiao Xue,* Xian Liu, Jianjie Fu, and Aiqian Zhang*

Cite This: *Environ. Health* 2025, 3, 133−142

Read Online

ACCESS | Metrics & More | Article Recommendations | Supporting Information

ABSTRACT: Fluorene-9-bisphenol (BHPF), emerging as an alternative to bisphenol A (BPA), is extensively utilized in industry and consumer goods. BHPF exhibits antiestrogenic effects and potential reproductive toxicity. Similar to BPA, BHPF can closely access the active site of the cytochrome P450 (CYP450) enzyme, interact with the Fe═O moiety, and potentially initiate metabolic reactions. Using density functional theory (DFT) calculations, we explored the mechanisms underlying BHPF activation using a CYP450 compound I (Cpd I) model, identifying several plausible products. Compared with the higher energy barriers associated with phenyl ring addition reactions, the formation of a phenoxyl-type radical through phenolic hydrogen atom abstraction, followed by OH rebound or radical coupling, represents an energetically favorable pathway. The OH rebound process yields three primary products: 9-(3,4-dihydroxyphenyl)-9-(4-hydroxyphenyl)fluorene (PRD1), semiquinone radical anion (PRD2), and 9-(4-hydroxyphenyl)fluorene carbocation (PRD3), constituting the major outcomes of the BHPF metabolic reaction. Importantly, a lipophilic ether metabolite, BHPF-O-BHPF (PRD4), formed through the coupling of phenoxyl radicals, reflects a widespread metabolic pathway observed in phenolic molecules. Despite constituting a minor proportion, the toxicity of this product necessitates increased attention. These findings contribute significantly to an enhanced understanding of the potential hazards associated with BHPF and other unknown chemical entities.

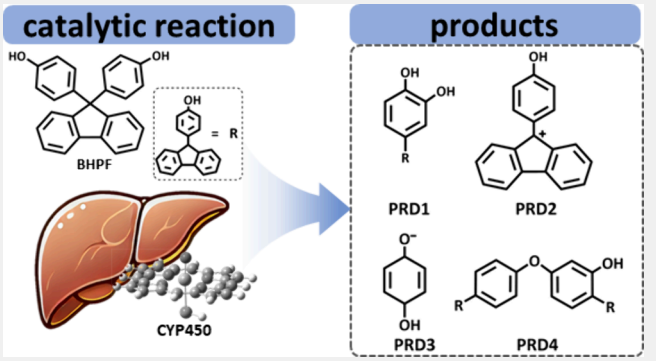

KEYWORDS: *fluorene-9-bisphenol, metabolism mechanism, CYP450, quantum chemical calculation, molecular docking*

INTRODUCTION

Bisphenol compounds, particularly bisphenol A (BPA), have been extensively used in producing polycarbonate and epoxy resins, which are commonly found in products such as baby bottles, plastic water bottles, and food storage containers.[1−3] Due to BPA's endocrine-disrupting properties, several developed countries have progressively banned or restricted its production and use.[4,5] As a novel alternative to BPA, fluorene-9-bisphenol (BHPF) has been widely adopted in protective coatings, semiconductor packaging, and medical devices due to its high thermal resistance. BHPF is also used in materials and containers that come into contact with food. Although BHPF was initially considered a safe alternative to BPA, recent research has identified it as an emerging environmental pollutant.[6,7] Studies have shown that BHPF can be released into aquatic environments and exhibits bioaccumulation. For example, Jin and Zhu detected BHPF concentrations of approximately 0.068 ng L^{-1} in the Liao River in Liaoning Province, China.[8] Despite the low concentrations of BHPF in natural water bodies, its continuous discharge and potential toxicity to organisms have raised significant concerns. Notably, due to BHPF's extensive use in food containers, its presence in human serum has been frequently reported. For example, Gao et al. detected BHPF in 80% of 353 individual serum samples.[9] Similarly, Lin et al. found BHPF in 14% of serum samples from pregnant women, with concentrations ranging from 1 to 100 nmol.[10] Their research also demonstrated that BHPF exposure led to programmed cell death in specific tissues of zebrafish, causing heart and vascular dysfunction. Additionally, BHPF exposure significantly altered antioxidant enzyme levels in mouse tests, indicating potential reproductive toxicity to mammals.[11]

Received: July 12, 2024
Revised: September 2, 2024
Accepted: September 3, 2024
Published: September 17, 2024

https://doi.org/10.1021/envhealth.4c00132
Environ. Health 2025, 3, 133−142

The structure of BHPF, which includes a fluorene group linked to two phenol groups, gives it a higher structural rigidity than BPA, resulting in different toxic effects. While BPA exhibits typical estrogen receptor-mediated estrogenic activity, BHPF displays antiestrogenic activity in both *in vitro* and *in vivo* studies with rodents, zebrafish, and Chinese medaka.[6,12,13] In 2020, Sun et al. found significant differences between the effects of BHPF and BPA on lipid metabolism in zebrafish.[14] BPA exposure led to lipid droplet accumulation and fat deposition in the liver, inducing nonalcoholic fatty liver disease and liver inflammation, whereas BHPF exposure had no significant effects on lipid metabolism.[15] Although both BHPF and BPA exposure reduced N^6-methyladenosine (m^6A) levels in zebrafish larvae RNA, the molecular mechanisms differ.[16] For example, BPA significantly increased the expression of the m6A reader *ythdf1*, while BHPF did not.[16] These differences may stem from their differential molecular recognition modes with target proteins, and metabolic transformation may also play an important role.

As a major phase I metabolic enzyme, cytochrome P450 (CYP450) plays a crucial role in the biotransformation of endogenous and exogenous compounds. Environmental pollutants catalyzed by CYP450 can undergo detoxification or produce more toxic intermediates or products, which may lead to an underestimation of the environmental and health risks of the pollutants. After being catalyzed by CYP450, BPA can generate metabolites with higher estrogenic activity, such as 4-hydroxycumyl alcohol (HCA) and 4-methyl-2,4-bis(p-hydroxyphenyl)pent-1-ene (MBP).[17,18] Considering the structural similarities between BHPF and BPA, the possibility that phase I metabolic transformation products lead to strong antagonistic effects on estrogen receptors cannot be completely ruled out. Unfortunately, there is currently no report on the systematic study of BHPF metabolic conversion. To scientifically assess the environmental and health risks of BHPF and ensure environmental safety and public health, it is imperative to systematically analyze the CYP450-mediated metabolic conversion mechanism of BHPF and elucidate its potential transformation products and reaction pathways. Conventional experimental methods have limitations and may not capture transient intermediates and transition states with extremely short lifespans during the reaction process. Using the CYP450 active center hexacoordinated tetravalent iron-oxygen-porphyrin complex Cpd I ($Fe^{4+}O^{2-}(C_{20}N_4H_{12})^-(SH)^-$) as an enzyme model, high-precision quantum chemical methods can help solve this problem. Cpd I has been successfully applied in evaluating the metabolic conversion of pollutants such as 2,2′,4,4′-tetrabromodiphenyl ether and triphenyl phosphate,[19−22] laying a good foundation for the computational evaluation of CYP450-mediated metabolic BHPF metabolic conversion. This study uses Cpd I as the enzyme model, selects appropriate functional and basis sets, and computationally evaluates the CYP450-mediated BHPF metabolic transformation process and possible products. The insights obtained through this computational approach are poised to enrich our understanding of BHPF's fate within biological systems and its potential implications for both the ecosystem and human health.

COMPUTATIONAL DETAILS

Molecular Docking

The molecular docking simulations were performed using the Autodock Vina program (version 1.2.5).[23,24] The CYP3A4 isoform, known for its high abundance and significant catalytic activity in the human body,[25−27] was employed as a plausible binding receptor for BHPF. The three-dimensional structure of human CYP3A4 (PDB code: 1tqn) was retrieved from the Protein Data Bank (https://www.rscsb.org/). Before the docking procedure was initiated, the binding ligands and water molecules present within CYP3A4 were manually removed. The receptor structure was prepared using the MGLTools software (version 1.5.6), where hydrogen atoms were added and Gasteiger charges were assigned. The ligand structure of BHPF were sourced from the PubChem database and prepared using the Open Babel software. The ligand was energy minimized by using the MMFF94 force field. During the binding process, CYP3A4 was maintained in a rigid state, while BHPF was treated as a flexible ligand. The binding pocket, with dimensions of 20 × 20 × 20 Å, was defined around the active site of CYP3A4. The default parameters of Autodock Vina were modified to increase docking accuracy: the exhaustiveness was set to 20 to ensure thorough sampling of the conformational space.

To ensure the reliability of the docking results, multiple docking runs (n = 5) were performed for each ligand (BHPF and BPA). The binding affinities for each docking run were recorded, and the mean and standard deviation of the binding affinities were calculated for both BHPF and BPA to assess the consistency and reliability of the docking scores. Key interactions, such as hydrogen bonds and hydrophobic contacts, between the ligands and the CYP3A4 enzyme were analyzed across multiple docking runs, and the frequency of these interactions was recorded to identify the most consistent and significant interactions.

Density Functional Theory (DFT) Calculations

In this section, we utilize a CYP450 enzyme active site model termed Cpd I to investigate the intricate mechanistic facets underpinning the biotransformation of BHPF. The molecular formula for this model is $Fe^{4+}O^{2-}(C_{20}N_4H_{12})^-(SH)$. Notably, previous studies have convincingly demonstrated the dependability and efficacy of this model in accurately describing the electronic structures and reactivity of CYP450 enzymes.[19−21,28] Given the closely located spin states of Cpd I, the energy profiles of various biotransformation pathways of BHPF were rigorously evaluated, considering both the high-spin (HS) quartet and low-spin (LS) doublet states. Examining both spin states allows for a comprehensive understanding of the potential mechanisms involved in the transformation of BHPF catalyzed by the CYP450 enzyme.

All DFT calculations were carried out using the Gaussian 16 software package.[29] The chosen density functional method was the hybrid functional Becke-3-parameter-Lee−Yang−Parr (B3LYP), known for its accurate representation of reaction mechanisms in CYP450 enzymes.[30] The DFT calculations involved the optimization of structures, frequency analyses, and single-point energy calculations for reaction compounds (RC), transition states (TS), intermediates (IM), and final products, all associated with various reaction pathways concerning BHPF biotransformation. To address the limitations of B3LYP in accurately describing dispersion interactions, the DFT-D3 empirical dispersion correction was incorporated into the calculations.[31,32]

The structural optimization and frequency analyses were conducted using the same computational level, denoted as BSI, with the Lanl2TZ(Fe)/6-31G**(H, C, N, O, S) basis set. For the single-point energy calculations of the optimized molecules, a higher-level basis set, BSII, was used. In this case, the Fe atom was computed using the Lanl2TZ(f) pseudopotential basis, while the H, C, N, O, and S atoms were treated with the 6-311++G** basis set. Furthermore, to consider the influence of the solvent environment on molecular energies during single-point energy calculations, the solvation model based on the density (SMD) was applied. Chlorobenzene (ε = 5.6), simulating a

https://doi.org/10.1021/envhealth.4c00132
Environ. Health 2025, 3, 133−142

weakly polar environment akin to the CYP450 enzyme interior, was chosen as the solvent for internal reactions.[30,33] For reactions occurring after the departure of the substance from CYP450, water (ε = 78.4) was selected as the solvent, representing the aqueous environment outside the enzyme cavity in a biological context. To account for changes in the zero-point vibration due to bond breaking and formation in the reactions, the zero-point correction (ZPE) was added to the final energies based on the single-point energy calculations. Additionally, intrinsic reaction coordinate (IRC) calculations were performed on the optimized transition states to verify their connectivity between reactants and products reliably. This approach offers a more robust evaluation than relying solely on imaginary frequencies to identify transition states.

To ensure the appropriateness of the chosen B3LYP functional for the target system, we performed a validation by comparing it with other density functional methods. Specifically, we compared the B3LYP results with those obtained using the Becke−Lee−Yang−Parr (BLYP), Becke−Perdew 1986 (BP86), Perdew−Burke−Ernzerhof (PBE), Tao−Perdew−Staroverov−Scuseria (TPSS), and Minnesota 2006 (M06) functionals. For this comparison, we conducted calculations for the H-abstraction and OH rebound reaction mediated by quartet Cpd I for BHPF. We assessed the sensitivity of the metabolic transformation reactions to the choice of density functional theory methods. All calculations were performed using the same BSI basis set and the DFT-D3 dispersion correction, and the SMD model was utilized in single-point energy calculations with chlorobenzene as the solvent. Furthermore, to evaluate the impact of the chosen basis set Lanl2TZ(f)(Fe)/6-311++G**(H, C, N, O, S) on the results, we performed a comparison with a more accurate all-electron def2-TZVP basis set (referred to as BSIII) in the context of the H-abstraction and OH rebound reactions of BHPF, with the DFT-D3 dispersion correction applied in the calculations as well.

RESULTS AND DISCUSSION

Docking Studies of BHPF and BPA with CYP3A4

Our investigation commenced by employing a widely used structure-based methodology, specifically molecular docking, to gain insights into the three-dimensional structures of protein-BHPF complexes and their underlying interactions. To facilitate a comparative analysis with the well-established endocrine disruptor BPA, we conducted molecular docking simulations of BPA with CYP3A4. Considering the crucial role of the heme Fe═O moiety within CYP enzymes, it is evident that substrate molecules must closely approach the reactive center to enable the ensuing chemical reactions. A fundamental empirical guideline, referred to as the "5 Å rule", postulates that potential sites for metabolism are located within a spatial range of 5 Å from the oxygen atom of the Fe = O moiety.

Based on molecular docking scoring, we identified the ten most favorable conformations of BHPF and BPA interacting with CYP3A4 (Figures S1 and S2). The binding energies and interatomic distances for these interactions are detailed in Table S1. For BPA the binding energies ranged from −6.4 to −7.3 kcal/mol with a mean value of −6.85 kcal/mol (±0.32). For BHPF, the binding energies ranged from −9.1 to −9.5 kcal/mol, with a mean value of −9.3 kcal/mol (±0.19). These results indicate that BHPF has a stronger and more favorable interaction with CYP3A4 compared to that of BPA.

We also analyzed the frequency of key interactions, such as hydrogen bonds and hydrophobic contacts, between the ligands and the CYP3A4 enzyme across multiple docking runs. The results are summarized in Table S2. The average closest interatomic distances between the heme group's oxygen atom and the ligands across the ten most favorable conformations were 5.54 Å for BPA and 5.01 Å for BHPF. The distances between the heme O moiety and the phenolic H atoms of BHPF and BPA in the closest conformations are 2.840 and 2.143 Å, respectively (Figure 1). These findings

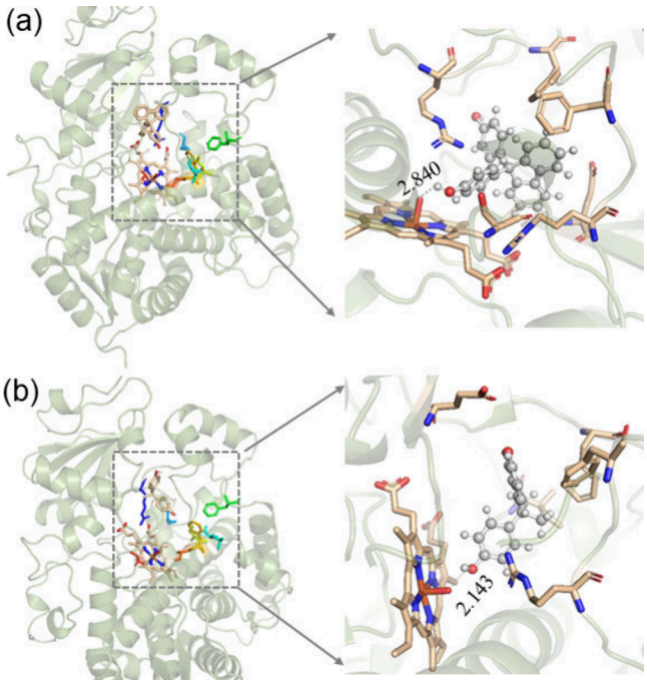

Figure 1. Molecular docking analysis of (a) BHPF and (b) BPA in the pocket of human CYP3A4 (PDB ID: 1tqn). Interactions between BHPF/BPA and the relevant amino acid residues are present in the docking conformations.

suggest that BHPF, akin to BPA, can readily penetrate the active site of the CYP450 enzyme. Moreover, the hydroxyl site of BHPF, characterized by the lowest interatomic distance to the heme O group, appears to be the most favorable region for facilitating the reaction. Based on these results, we can conclude that BHPF is likely to be efficiently metabolized by CYP3A4, potentially leading to the formation of reactive intermediates.

Biotransformation Profiles of BHPF by CYP450

DFT Method Comparison. To determine the most suitable density functional theory method for this study, six distinct methods, namely, B3LYP, BLYP, BP86, PBE, TPSS, and M06, were employed to conduct calculations on the hydrogen abstraction and OH-rebound reactions of BHPF mediated by Cpd I in the quadruplet state. The intricate molecular mechanism is expounded upon in the subsequent sections, wherein the intermediate and transition states participated in the reactions are denoted as ^{4}RC, ^{4}TS7, ^{4}IM7, ^{4}TS8, and ^{4}IM8. Upon meticulous examination of the transition state configurations obtained using the six functional methods (Figure S3), it becomes evident that a remarkable agreement exists in the critical bond lengths, indicating the attainment of similar geometric structures across all six methods. Specifically, during the hydrogen abstraction step, the variation in the O−H bond length of the phenolic hydroxyl group in the BHPF molecule is confined to a narrow range of 1.162−1.214 Å, exhibiting a mere maximum deviation of 0.052 Å. This observation suggests that the optimized configurations obtained by the six functional methods exhibit minimal

https://doi.org/10.1021/envhealth.4c00132
Environ. Health 2025, 3, 133−142

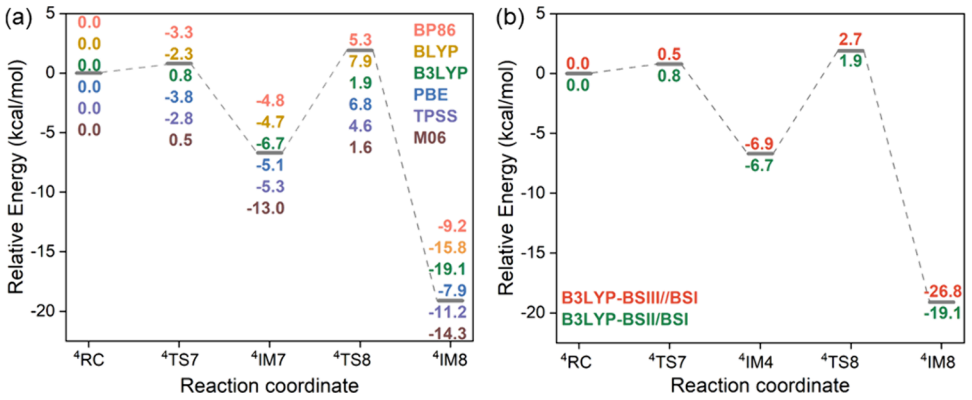

Figure 2. Reaction profiles for the reactions of H-abstraction−OH-rebound path of BHPF mediated by Cpd I calculated with six DFT functional methods (a) and two basis sets (b).

differences, reinforcing the reliability and accuracy of the results obtained from these computational approaches.

Figure 2a presents the potential energy profiles calculated by using the six functional methods. Evidently, the hydrogen abstraction step in the BHPF reactions catalyzed by Cpd I manifests a relatively low energy barrier. Specifically, the B3LYP and M06 methods yield energy barriers of 0.8 and 0.5 kcal/mol, respectively, indicating the relatively facile nature of this step. In contrast, the BP86, BLYP, PBE, and TPSS methods yield negative values for the reaction energy barriers. Notably, the BP86, PBE, and BLYP methods belong to the generalized gradient approximation (GGA) family, employing electronic density and its gradient as variables.[34] The TPSS method, categorized as a meta-GGA method, also encounters challenges in accurately describing the hydrogen transfer intrinsic.[35] Conversely, the B3LYP and M06 methods, functioning as hybrid functional incorporating Hartree−Fock exchange-correlation terms, provide more precise descriptions of this reaction and yield reasonable results for the reaction potential energy barriers.[36] These findings underscore the significance of employing appropriate theoretical methods, such as hybrid functionals, to gain reliable insights into the mechanistic details of hydrogen abstraction reactions in the context of CYP450 enzyme catalysis. Nevertheless, it is important to highlight that the M06 functional may overestimate the stability of high-spin state compounds in ferrous heme model calculations.[37] For instance, the ^{4}IM7 computed using the B3LYP method lies 6.7 kcal/mol below the reactant intermediate ^{4}RC, while the ^{4}IM7 obtained with the M06 functional is at −13.0 kcal/mol, resulting in a significantly higher activation energy of 14.6 kcal/mol for the OH rebound step under the M06 method, as opposed to the 8.6 kcal/mol calculated by B3LYP. Therefore, we chose the B3LYP functional to assess the metabolic transformation process of BHPF mediated by CYP450.

Upon selection of the B3LYP functional, we conducted a thorough assessment of the influence of the basis set on the energy variation along this pathway. Specifically, two basis sets were considered: the Lanl2TZ(f)(Fe)/6-311++G**(H, C, N, O, S) basis set (BSII) and the more accurate all-electron def2-TZVP basis set (BSIII). The potential energy surface profile (Figure 2b) indicates that although there are slight disparities in the absolute energy values obtained using the two basis sets for this reaction pathway, the overall trends remain consistent. Furthermore, taking into account the higher computational efficiency of the BSII basis set compared with the all-electron BSIII basis set, we opted to utilize the BSII basis set for subsequent computational evaluations in this study.

Initial Reaction Mechanisms of CYP450-Catalyzed BHPF. In general, CYP450 catalyzes reactions involving biphenolic compounds through two distinct mechanisms. The first mechanism encompasses the direct addition of the iron-oxo moiety of Cpd I to the benzene ring of the biphenolic substrate, facilitated by p−π bonding. The second one entails the oxo group of Cpd I abstracting a hydrogen atom from the phenolic ring, as illustrated in Figure 3. The O-addition

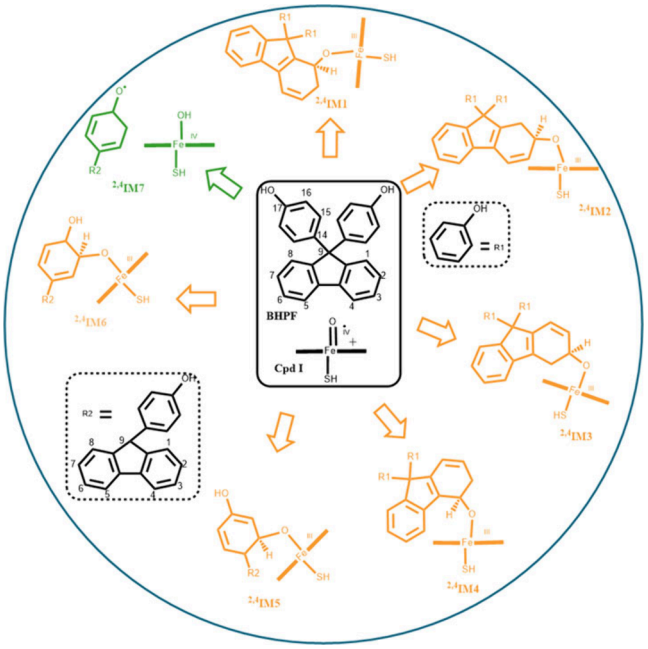

Figure 3. Viable initial reaction mechanisms of BHPF catalyzed by P450 Cpd I explored in this study. The green color indicates the H-abstraction pathway, and the orange paths depict the O-addition reactions.

reactions can transpire at four carbon sites on the fluorene ring, designated as paths 1−4, or P1−P4, as well as at two carbon sites on the phenol ring, denoted as paths 5 and 6 (or P5 and P6). During this process, the oxo moiety of Cpd I undergoes a transformation from sp^2 to sp^3 hybridization, whereby the newly formed sp^3 hybrid orbital aligns in a "head-to-head" manner with the C atom p orbital of the BHPF molecule. This

https://doi.org/10.1021/envhealth.4c00132
Environ. Health 2025, 3, 133−142

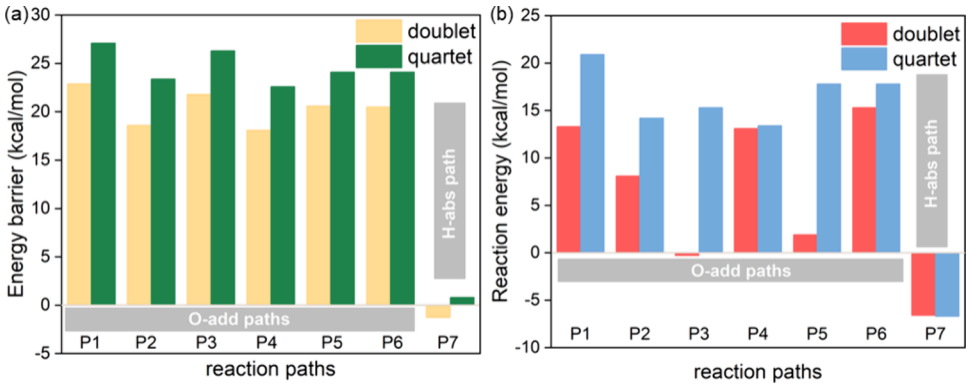

Figure 4. Energy barriers and reaction energy changes involved in the initial reactions of BHPF catalyzed by P450 Cpd I.

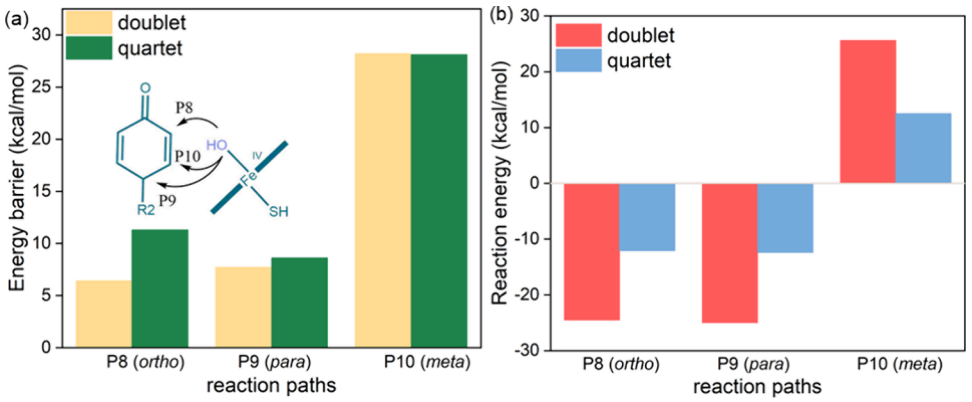

Figure 5. Energy barriers and reaction energy changes involved in the OH-rebound reactions of IM7.

alignment leads to the establishment of a new σ bond via a tetrahedral transition state. Energy barriers and reaction energy changes for the initial reaction paths are presented in Figure 4, with the corresponding potential energy surfaces being depicted in Figure S4. It is evident from the figures that the oxygen addition reactions are characterized by notably elevated energy barriers, ranging from 18.1 to 26.3 kcal/mol, on both the doublet and the quartet state surfaces. Additionally, nearly all of these reactions exhibit endothermic behavior, which indicate the greater instability of the newly formed adducts compared to the initial reactants. These outcomes are consistent with earlier investigations into CYP450-mediated BPA metabolic transformation reactions.[38] It has been reported that the barriers for oxygen addition to the *ortho*- and *meta*-carbon sites are 14.4/17.5 and 17.0/19.9 kcal/mol, respectively, on the quartet/doublet state surfaces, signifying the presence of relatively substantial barriers. Thus, for both BPA and BHPF, oxygen addition reactions require substantial energy input and are less favorable from both thermodynamic and kinetic perspectives. This may be attributed to the formation of a tetrahedral configuration at the attacked C atom after the formation of the new σ bond, disrupting the large π bond structures of the fluorene or benzene ring and thereby increasing the activation energy for oxygen addition.

Conversely, the H abstraction pathway of Cpd I involves the approach of the Fe−O group toward the hydroxyl hydrogen atom of BHPF. This process leads to the creation of nearly linear transition states, termed as ^{2}TS7 and ^{4}TS7, characterized by O··H··O configurations. Ultimately, the oxo moiety of Cpd I captures the hydrogen atom, giving rise to the formation of a porphyrin-iron-hydroxyl complex (referred to as Cpd II) in conjunction with the BHPF phenoxyl radical (labeled as BHPFR). This sequence culminates in the generation of intermediates ^{2}IM7 and ^{4}IM7. As illustrated in Figure 3 and Figure S4, the H-abstraction barrier is minimal, measuring 0.8/−1.2 kcal/mol for the quartet/doublet state. This barrier magnitude is similar to the slight barriers observed for the phenolic group of BPA and paracetamol molecules.[38,39] Additionally, the resultant complex intermediates (^{2}IM7 and ^{4}IM7) exhibit stability, characterized by exothermic reaction energies of −6.7/−6.6 kcal/mol for the quartet/doublet state. These findings demonstrate that analogously to the metabolic reactions of BPA, the H-abstraction pathway functions as the primary initiation route.

OH Rebound of Phenoxyl-Type Radical Intermediate IM7 and Subsequent Decomposition Reactions. As outlined in the preceding section, following the abstraction of the phenolic hydrogen atom from BHPF by the oxo moiety of Cpd I, a pivotal intermediate complex emerges, characterized by triplet state compound II (Cpd II) along with a BHPF phenoxyl radical. The BHPF phenoxyl radical possesses an unpaired electron that can be delocalized over the phenolic oxygen atom and the carbon atom of the phenolic benzene ring. Consequently, this phenomenon results in an increased electron density, particularly at the *ortho*- and *para*-carbon positions. Subsequently, the lone pair electron associated with the iron-hydroxo species in Cpd II readily aligns with the carbon p orbitals of the benzene ring, adopting a "head-to-head" manner. This alignment facilitates the creation of a new σ bond, which rebounds to the *ortho*-, *para*-, or *meta*-carbons of the benzene ring (denoted as paths 8−10, or P8−P10), leading to the production of quinol intermediates. The energy

https://doi.org/10.1021/envhealth.4c00132
Environ. Health 2025, 3, 133−142

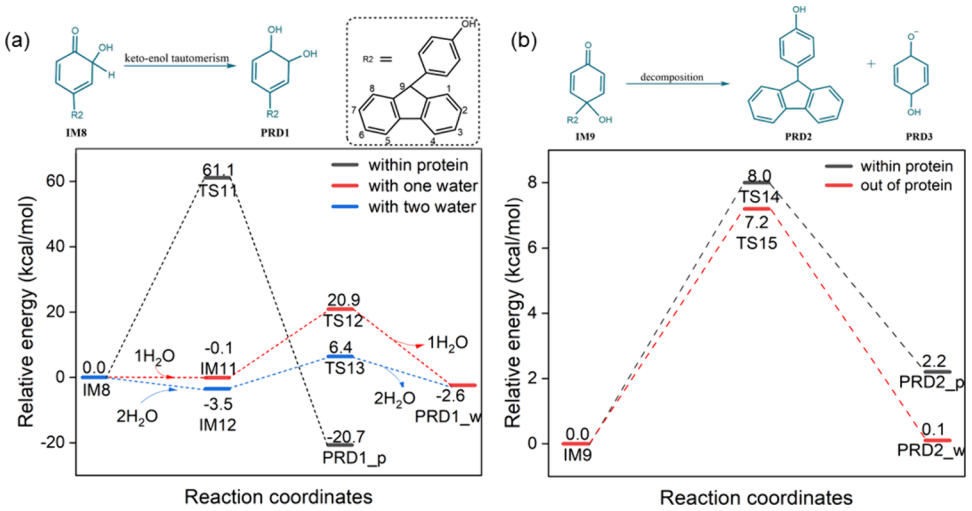

Figure 6. Reaction schemes and energy profiles for the subsequent reactions of M8 (a) and IM9 (b).

barriers and reaction energy changes for the hydroxyl rebound process are graphically illustrated in the column chart depicted in Figure 5. Moreover, the corresponding potential energy surfaces are presented in Figure S5. Notably, the energy barriers for OH rebound to the *ortho*- and *para*-carbons are found to be 11.3/6.4 and 8.6/7.7 kcal/mol, respectively, in the quartet/doublet states. Furthermore, the OH-rebound reactions occurring at both the *ortho*- and *para*-positions are exothermic, with respective values of 12.1/24.5 and 12.4/25.0 kcal/mol in the quartet/doublet states, indicative of spontaneous processes. However, the energy barriers for the rebound reaction at the *meta*-carbon are considerably higher, measuring 28.2 and 28.1 kcal/mol in the quartet/doublet states. In a previous study, Ji et al.[31] reported that the energy barriers for hydroxyl rebound to the *para* and *ortho* carbon atoms of the BPA were significantly lower than those associated with the *meta* rebound processes. These findings underscore that for both BPA and BHPF, the *para* and *ortho* rebound pathways are favored in the OH rebound process following the formation of the phenoxyl radical, while the *meta* rebound process is marked as unfavorable from both thermodynamic and kinetic standpoints.

In reference to the study conducted by Ji et al.[38] concerning the metabolic mechanisms of a BPA molecule, it is posited that analogous metabolic reactions occur with regard to BHPF, extending beyond the quinol intermediates IM8−IM10. Given the significant energy barrier associated with the *meta* rebound phenomenon, our attention is directed solely toward the subsequent reaction pathways of the intermediates IM8 and IM9, situated at the *para* and *ortho* positions, respectively. Upon the occurrence of hydroxyl rebound at the neighboring carbon atom, a tetrahedral configuration is established in conjunction with the hydrogen atom originally bonded to the carbon atom. To attain a stable benzene ring structure, the previously bound hydrogen atom exhibits a preference for transferring to the carbonyl oxygen atom via keto−enol tautomerization. It is noteworthy that this rearrangement process does not necessitate the involvement of the CYP450 active center. Instead, it can take place within the enzyme's hydrophobic cavity through direct hydrogen atom translocation or, once the intermediate exists, the enzyme pocket into an aqueous environment, facilitated by water molecules acting as bridges. To this end, distinct solvent systems, specifically chlorobenzene and water, were employed to respectively simulate the enzyme cavity's hydrophobic environment and the aqueous environment beyond it. Computational analyses were carried out on the IM8 reaction within these distinct environments.

Depicted in Figure 6a is the energy profile of keto−enol tautomerization during the *ortho* hydroxyl rebound. The figure shows that within the enzyme's hydrophobic cavity, the isomerization reaction involving direct hydrogen transfer proceeds through a four-membered-ring transition state. The significant ring strain in this transition state results in a high reaction energy barrier of 60.6 kcal/mol. Given the difficulty of achieving such elevated energy levels within a biological context, this reaction pathway is virtually implausible. However, when this intermediate exits the enzyme cavity and enters an aqueous environment, the formation of a hydrogen bond network with the assistance of water molecules facilitates the reaction. For instance, the involvement of one water molecule can form a six-membered-ring transition state, significantly reducing the ring strain and lowering the reaction energy barrier to 27.6 kcal/mol. With the assistance of two water molecules, an eight-membered-ring transition state is formed, further reducing the reaction energy barrier to 9.9 kcal/mol. Importantly, both processes involving one or two water molecules as bridges exhibit highly exothermic characteristics, with reaction energy values of −18.0 and −22.4 kcal/mol, respectively. Consequently, it becomes evident that the keto−enol tautomerization process of the *ortho*-hydroxyl rebound intermediate can occur spontaneously beyond the enzyme's cavity within a biological system, leading to the generation of 9-(3,4-dihydroxyphenyl)-9-(4-hydroxyphenyl)-fluorene (PRD1).

In contrast, intermediate IM9, arising from *para* hydroxyl rebound, tends to undergo decomposition reactions, resulting in the production of hydroquinone and 4-(9-fluorenylidene) phenol. As depicted in Figure 6b, IM9 is capable of undergoing a self-decomposition reaction, leading to the formation of a semiquinone radical anion (PRD2) and a 9-(4-hydroxyphenyl)fluorene carbocation (PRD3). The energy barriers required for these transitions within the protease pocket and in the aqueous environment outside the enzyme pocket are quantified at 8.0 and 7.2 kcal/mol, respectively. Both barriers correspond to processes characterized by low

https://doi.org/10.1021/envhealth.4c00132
Environ. Health 2025, 3, 133−142

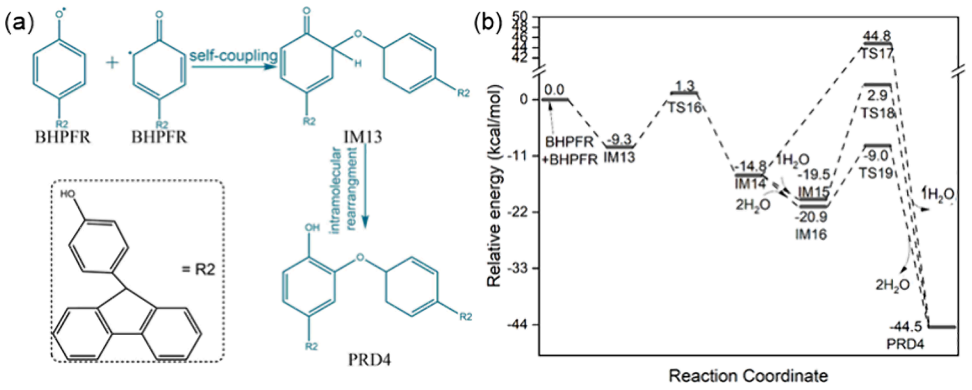

Figure 7. Reaction scheme (a) and energy profiles (b) for the coupling reactions of BHPFR.

endothermicity, entailing the absorption of 2.2 and 0.1 kcal/mol of heat, sequentially.

Self-Coupling Reactions of BHPF Phenoxyl Radical: Formation of Ether-Type Product. Initiated by the hydrogen abstraction process in Figure 3, it becomes evident that the transfer of the hydroxyl hydrogen atom from BHPF to the Fe═O moiety of Cpd I gives rise to the formation of triplet state Cpd II and the BHPF phenoxyl radical. This progression is characterized by negligible energy barriers involved in either quartet or doublet state. Notably, the resultant triplet state Cpd II can interact further with other organic molecules entering the protein cavity. Specifically, it can abstract an addition hydroxyl hydrogen atom from a distinct BHPF molecule, thereby generating a new phenoxyl-type radical. This reaction necessitates surmounting a relatively minor energy barrier of 4.4 kcal/mol and results in the liberation of 7.2 kcal/mol of the reaction heat (Figure S6). Evidently, both Cpd I and Cpd II possess the capacity to catalyze hydrogen abstraction reactions within conventional biphenolic compounds, ultimately yielding the emergence of phenoxyl radicals. Similar conclusions have been drawn from computational studies on the CYP450-mediated trichlorosilane coupling reaction, wherein both Cpd I and Cpd II effectively catalyze the generation of phenoxyl radicals through the process of hydrogen abstraction.[40] This underscores the robust capability of CYP450 to facilitate the hydrogen abstraction of phenolic hydroxyl hydrogen atoms and engender the formation of phenoxyl radicals. It is crucial to underscore that the generated phenoxyl-type radicals, beyond undergoing the rebound reactions, possess the capacity to engage in mutual coupling, resulting in the formation of ether compounds.

To gain further insight into the structural basis of the ensuing coupling reactions involving the BHPF phenoxyl radical, Figure S7 depicts the spatial distribution of spin density for the BHPF phenoxyl radical. As observed from Figure S7, the allocation of unpaired electrons resulting from the process of hydrogen abstraction reveals a delocalized distribution that encompasses specific regions, specifically the hydroxyl oxygen atom, as well as the *ortho*- and *para*-carbon positions of the phenyl ring within the generated BHPF phenoxyl radical. This observation effectively designates these specific locations as potential reaction sites for the BHPF phenoxyl radical. As a result, the plausible modes of radical coupling involving the BHPF phenoxyl radical encompass the O−O, O−C, and the C−C coupling. Given the inherent instability linked with the O−O coupling leading to peroxide formation, along with the elevated energy barriers associated with C−C coupling, this study exclusively focuses on C−O coupling. Specifically, the focal point is the electrophilic assault of the hydroxyl oxygen atom of BHPF onto the *ortho*- or *para*-carbon center of another radical. It is worth noting that the reaction at the *para*-carbon atom site encounters significant steric hindrance. Therefore, this study primarily analyzes the O−C_{ortho} radical coupling reaction.

The coupling of two BHPF phenoxy radicals can potentially occur inside the protein cavity or in an aqueous environment outside the cavity. We first conducted molecular docking of the O−C_{ortho} ether coupling product with the CYP450 enzyme (PDB code: 1tqn) and compared it with the molecular docking results of the BHPF-O-phenol ether product. Our study found that the binding energy of BHPF-O-BHPF with the CYP450 enzyme is 13 kcal/mol, whereas the binding energy of BHPF-O-phenol with CYP450 is −10.3 kcal/mol. This result indicates that the limited volume of the enzyme cavity makes it difficult to accommodate two BHPF phenoxy radicals. Therefore, it is reasonable to infer that the radical−radical coupling reaction of BHPF occurs in an aqueous environment outside the protein cavity. The schematic representation of the O−C_{ortho} coupling reaction pathway between two BHPF phenoxyl radicals and the corresponding potential energy surface profiles are depicted in Figure 7. From the diagram, it can be observed that one BHPF phenoxyl radical (BHPFR) engages in an attack on the adjacent carbon atom of another BHPFR's oxygen center, resulting in the formation of a coupled adduct with an energy barrier of 10.6 kcal/mol. The attacked carbon atom adopts a tetrahedral configuration. Subsequent intramolecular rearrangement of the coupled adduct leads to the formation of a lipophilic ether metabolite, BHPF-O-BHPF (PRD4). The potential energy surface profiles reveal that a direct molecular rearrangement entails a high energy barrier of 59.6 kcal/mol. However, with the collaborative influence of water molecules, the reaction barrier can be significantly reduced to 22.4 and 11.9 kcal/mol, accompanied by a substantial release of heat (44.5 kcal/mol) during the formation of the final product.

Toxicity Assessment during the Metabolic Transformation of BHPF. In this section, we evaluate the toxicity changes of BHPF after metabolic transformation. Upon catalysis by CYP450, BHPF primarily generates four metabolites: PRD1−PRD4. PRD1 is an *ortho*-hydroxylated product that has also been detected in the metabolic pathways of other bisphenol compounds. This metabolite can further oxidize to form *ortho*-quinone. Previous studies have demonstrated that *ortho*-quinone products formed after BPA

https://doi.org/10.1021/envhealth.4c00132
Environ. Health 2025, 3, 133−142

metabolism can bind to MCF-7 cell DNA, indicating that the quinone metabolites of BHPF might similarly covalently bind to DNA, presenting potential carcinogenic risks.[41−43] PRD2 and PRD3 are derived from the *para*-rebound intermediate, decomposing into carbocation PRD2 and hydroquinone PRD3. Although the toxicological effects of PRD2 have not yet been investigated, it is important to note that PRD3 hydroquinone is recognized as a potential carcinogen.[44] Furthermore, the coupling of two phenoxy radicals results in the formation of ether metabolite PRD4. It is noteworthy that the dimerization and coupling reaction pathways of phenolic compounds are prevalent in the metabolism of phenolic hydroxyl-containing substances.[45,46] For instance, triclosan (TCS), after transformation by CYP450 enzymes, produces a coupling product that exhibits stronger binding activity to androgen receptors compared to the parent compound TCS.[45] This observation suggests that the high molecular weight BHPF-O-BHPF, formed postmetabolism, may have a higher propensity to bind to biomolecules, thereby inducing toxic effects or accumulating within organisms. In other words, the metabolites of BHPF may exhibit greater toxicity than the parent compound itself, warranting further investigation and attention.

CONCLUSIONS

In conclusion, this study provides a comprehensive exploration of the molecular mechanisms underlying the metabolism of BHPF by CYP450 enzymes and proposes potential reaction products. Our results highlight the ability of BHPF to access the active site of CYP450 enzymes, similar to BPA, facilitating enzymatic metabolic reactions. The primary mode of the reaction for BHPF involves a hydrogen abstraction pathway mediated by Cpd I, leading to the formation of three distinct products: 9-(3,4-dihydroxyphenyl)-9-(4-hydroxyphenyl)-fluorene (PRD1), semiquinone radical anion (PRD2), and 9-(4-hydroxyphenyl)fluorene carbocation (PRD3). Notably, the phenoxyl radical formed after hydrogen abstraction can engage in self-coupling reactions, resulting in the formation of the ether compound BHPF-O-BHPF (PRD4). These findings not only enhance our comprehension of BHPF metabolism but also emphasize the importance of considering BHPF and its metabolites as potential environmental contaminants. These insights are pivotal for assessing and mitigating the ecological impact of BHPF, thereby contributing to more informed environmental management strategies and policies. Further research should focus on experimentally validating these pathways and evaluating the long-term ecological and health effects of BHPF and its metabolites.

ASSOCIATED CONTENT

Supporting Information

The Supporting Information is available free of charge at https://pubs.acs.org/doi/10.1021/envhealth.4c00132.

The ten most favorable conformations of BHPF and BPA interacting with CYP3A4, optimized geometries of ^{4}TS7 and ^{4}TS8 calculated with six functional methods, reaction profiles for initial reactions of BHPF catalyzed by P450 Cpd I, reaction profiles for OH-rebound reactions of IM7, reaction energy profiles for H-abstraction reaction of BHPF catalyzed by Cpd II, spin density distribution of BHPFR radical, closest interatomic distance (in Å) of the ten most favorable configurations of BHPF/BPA within CYP3A4 (PDB ID: 1TQN) and the corresponding binding affinity (in kcal/mol), statistical analysis of binding energies, and the Cartesian coordinates of the optimized geometries for the reactants, products, intermediates, and transition state structures involved in this study (PDF)

AUTHOR INFORMATION

Corresponding Authors

Qiao Xue − *State Key Laboratory of Environmental Chemistry and Ecotoxicology, Research Center for Eco-Environmental Sciences, Chinese Academy of Sciences, Beijing 100085, China;* orcid.org/0000-0002-0325-9996; Email: qiaoxue@rcees.ac.cn

Aiqian Zhang − *State Key Laboratory of Environmental Chemistry and Ecotoxicology, Research Center for Eco-Environmental Sciences, Chinese Academy of Sciences, Beijing 100085, China; School of Environment, Hangzhou Institute for Advanced Study, University of Chinese Academy of Sciences, Hangzhou 310012, China; College of Resources and Environment, University of Chinese Academy of Sciences, Beijing 100049, China;* orcid.org/0000-0001-5680-2529; Email: aqzhang@rcees.ac.cn

Authors

Wenxiao Pan − *State Key Laboratory of Environmental Chemistry and Ecotoxicology, Research Center for Eco-Environmental Sciences, Chinese Academy of Sciences, Beijing 100085, China;* orcid.org/0000-0002-9719-4467

Shuming He − *School of Environment, Hangzhou Institute for Advanced Study, University of Chinese Academy of Sciences, Hangzhou 310012, China*

Yinzheng Yang − *School of Environment, Hangzhou Institute for Advanced Study, University of Chinese Academy of Sciences, Hangzhou 310012, China*

Yongdie Yang − *State Key Laboratory of Environmental Chemistry and Ecotoxicology, Research Center for Eco-Environmental Sciences, Chinese Academy of Sciences, Beijing 100085, China; College of Resources and Environment, University of Chinese Academy of Sciences, Beijing 100049, China*

Xian Liu − *State Key Laboratory of Environmental Chemistry and Ecotoxicology, Research Center for Eco-Environmental Sciences, Chinese Academy of Sciences, Beijing 100085, China;* orcid.org/0000-0002-5398-4707

Jianjie Fu − *State Key Laboratory of Environmental Chemistry and Ecotoxicology, Research Center for Eco-Environmental Sciences, Chinese Academy of Sciences, Beijing 100085, China; School of Environment, Hangzhou Institute for Advanced Study, University of Chinese Academy of Sciences, Hangzhou 310012, China; College of Resources and Environment, University of Chinese Academy of Sciences, Beijing 100049, China;* orcid.org/0000-0002-6373-0719

Complete contact information is available at: https://pubs.acs.org/10.1021/envhealth.4c00132

Author Contributions

W.P.: investigation, visualization, writing−original draft. S.H.: methodology, software, writing−review and editing. Yinzheng Yang: validation. Q.X.: conceptualization, writing−review and editing. X.L. and J.F.: supervision. A.Z.: conceptualization,

writing−review and editing. All authors have given approval for the final version of the paper.

Notes

The authors declare no competing financial interest.

■ ACKNOWLEDGMENTS

This research was jointly supported by the projects of the National Key Research and Development Program of China (2020YFA0907500 and 2021YFC3200101), the projects of National Natural Science Foundation of China (22193053, 22276197, and 22136001), the Youth Innovation Promotion Association of CAS (Y2022020), and the Strategic Priority Research Program of the Chinese Academy of Sciences (XDB0750100).

■ REFERENCES

(1) Wilson, N. K.; Chuang, J. C.; Morgan, M. K.; Lordo, R. A.; Sheldon, L. S. An observational study of the potential exposures of preschool children to pentachlorophenol, bisphenol-A, and nonylphenol at home and daycare. *Environ. Res.* **2007**, *103*, 9−20.

(2) Geens, T.; Aerts, D.; Berthot, C.; Bourguignon, J. P.; Goeyens, L.; Lecomte, P.; Maghuin-Rogister, G.; Pironnet, A. M.; Pussemier, L.; Scippo, M. L.; Van Loco, J.; Covaci, A. A review of dietary and non-dietary exposure to bisphenol-A. *Food Chem. Toxicol.* **2012**, *50*, 3725−3740.

(3) Dai, Z.; Li, Y.; Yang, S.; Zhao, N.; Zhang, X.; Xu, J. Kinetics and thermal properties of epoxy resins based on bisphenol fluorene structure. *Eur. Polym. J.* **2009**, *45*, 1941−1948.

(4) Moreman, J.; Lee, O.; Trznadel, M.; David, A.; Kudoh, T.; Tyler, C. R. Acute toxicity, teratogenic, and estrogenic effects of bisphenol A and its alternative replacements bisphenol S, bisphenol F, and bisphenol AF in zebrafish embryo-larvae. *Environ. Sci. Technol.* **2017**, *51*, 12796−12805.

(5) den Braver-Sewradj, S. P.; van Spronsen, R.; Hessel, E. V. S. Substitution of bisphenol A: A review of the carcinogenicity, reproductive toxicity, and endocrine disruption potential of alternative substances. *Crit. Rev. Toxicol.* **2020**, *50*, 128−147.

(6) Fan, X.; Guo, J.; Jia, X.; Mao, X.; Zhou, Y.; Wang, Y.; Guo, X.; Shen, J.; Huai, N.; Zhang, K.; Abdusalam, A.; Hu, H.; Zhu, H.; Jia, C.; Cheng, L.; Li, X.; Zhang, Z. Reproductive toxicity and teratogenicity of fluorene-9-bisphenol on chinese medaka (oryzias sinensis): A study from laboratory to field. *Environ. Sci. Technol.* **2023**, *57*, 561−569.

(7) Liu, X.; Cheng, Z.; Shang, X.; Zhang, H.; Liu, X.; Pan, W.; Fu, J.; Xue, Q.; Zhang, A. New mechanism for the apoptosis of human neuroblastoma cells by the interaction between fluorene-9-bisphenol and the G protein-coupled estrogen receptor 1. *Environ. Sci. Technol.* **2024**, *58*, 10494−10503.

(8) Jin, H.; Zhu, L. Occurrence and partitioning of bisphenol analogues in water and sediment from Liaohe river basin and Taihu lake. *China. Water Res.* **2016**, *103*, 343−351.

(9) Gao, C. Z.; He, H. H.; Qiu, W. H.; Zheng, Y.; Chen, Y. Y.; Hu, S. Y.; Zhao, X. Oxidative stress, endocrine disturbance, and immune interference in humans showed relationships to serum bisphenol concentrations in a dense industrial area. *Environ. Sci. Technol.* **2021**, *55*, 1953−1963.

(10) Lin, J. B.; Zhan, G. K.; Liu, J. F.; Maimaitiyiming, Y.; Deng, Z. P.; Li, B. H.; Su, K. H.; Chen, J. F.; Sun, S. Q.; Zhen, W. L.; Yu, X. H.; He, F.; Cheng, X. D.; Wang, L. F.; Shen, B.; Yao, Z. Q.; Yang, X. Q.; Zhang, J.; He, W. T.; Wu, H. Y.; Naranmandura, H.; Chang, K. J.; Min, J. X.; Ma, J.; Björklund, M.; Xu, P. F.; Wang, F.; Hsu, C. H. YTHDF2-mediated regulations bifurcate BHPF-induced programmed cell deaths. *Natl. Sci. Rev.* **2023**, *10*, No. nw23.

(11) Feng, Q.; Liu, Y.; Zou, L.; Lei, M.; Zhu, C.; Xia, W. Fluorene-9-bisphenol exposure damages the testis in mice through a novel mechanism of ferroptosis. *Food Chem. Toxicol.* **2024**, *184*, No. 114385.

(12) Zhang, Z.; Hu, Y.; Guo, J.; Yu, T.; Sun, L.; Xiao, X.; Zhu, D.; Nakanishi, T.; Hiromori, Y.; Li, J.; Fan, X.; Wan, Y.; Cheng, S.; Li, J.; Guo, X.; Hu, J. Fluorene-9-bisphenol is anti-oestrogenic and may cause adverse pregnancy outcomes in mice. *Nat. Commun.* **2017**, *8*, 14585.

(13) Mi, P.; Zhang, Q. P.; Zhang, S. H.; Wang, C.; Zhang, S. Z.; Fang, Y. C.; Gao, J. Z.; Feng, D. F.; Chen, D. Y.; Feng, X. Z. The effects of fluorene-9-bisphenol on female zebrafish (danio rerio) reproductive and exploratory behaviors. *Chemosphere* **2019**, *228*, 398−411.

(14) Sun, L.; Ling, Y.; Jiang, J.; Wang, D.; Wang, J.; Li, J.; Wang, X.; Wang, H. Differential mechanisms regarding triclosan vs. bisphenol A and fluorene-9-bisphenol induced zebrafish lipid-metabolism disorders by RNA-seq. *Chemosphere* **2020**, *251*, 126318.

(15) Zhang, Y. X.; Yan, C. C.; Xie, Q.; Wu, B.; Zhang, Y. C. Exposure to bisphenol A affects transcriptome-wide N6-methyladenine methylation in ovarian granulosa cells. *Ecotoxicol. Environ. Saf.* **2024**, *272*, 116071.

(16) Ling, Y.; Huang, X.; Li, A.; Zhang, J.; Chen, J.; Ren, J.; Liu, Y.; Xie, M. Bisphenol A exposure induces testicular oxidative damage via FTO/m6A/Nrf2 axis during postnatal development in mice. *J. Appl. Toxicol.* **2023**, *43*, 694−705.

(17) Nakamura, S.; Tezuka, Y.; Ushiyama, A.; Kawashima, C.; Kitagawara, Y.; Takahashi, K.; Ohta, S.; Mashino, T. Ipso substitution of bisphenol A catalyzed by microsomal cytochrome P450 and enhancement of estrogenic activity. *Toxicol. Lett.* **2011**, *203*, 92−95.

(18) Yoshihara, S.; Mizutare, T.; Makishima, M.; Suzuki, N.; Fujimoto, N.; Igarashi, K.; Ohta, S. Potent estrogenic metabolites of bisphenol A and bisphenol B formed by rat liver S9 fraction: Their structures and estrogenic potency. *Toxicol. Sci.* **2004**, *78*, 50−59.

(19) Fu, Z.; Wang, Y.; Chen, J.; Wang, Z.; Wang, X. How PBDEs are transformed into dihydroxylated and dioxin metabolites catalyzed by the active center of cytochrome P450s: A DFT Study. *Environ. Sci. Technol.* **2016**, *50*, 8155−8163.

(20) Wang, X.; Wang, Y.; Chen, J.; Ma, Y.; Zhou, J.; Fu, Z. Computational toxicological investigation on the mechanism and pathways of xenobiotics metabolized by cytochrome P450: A case of BDE-47. *Environ. Sci. Technol.* **2012**, *46*, 5126−5133.

(21) Zhang, Q.; Ji, S.; Chai, L.; Yang, F.; Zhao, M.; Liu, W.; Schüürmann, G.; Ji, L. Metabolic mechanism of aryl phosphorus flame retardants by cytochromes P450: A combined experimental and computational study on triphenyl phosphate. *Environ. Sci. Technol.* **2018**, *52*, 14411−14421.

(22) Wang, W.; Gao, Y. P.; Luo, N.; Chen, G. H.; Niu, X. L.; Li, G. Y.; An, T. C. 1-Nitropyrene metabolism and health risk: Identification of key enzymes, pathways, and metabolites using a multimethod approach. *Environ. Health* **2023**, *1*, 383−393.

(23) Trott, A. J.; Olson, A. AutoDock Vina: Improving the speed and accuracy of docking with a new scoring function, efficient optimization, and multithreading. *J. Comput. Chem.* **2010**, *31*, 455−461.

(24) Xue, Q.; Liu, X.; Russell, P.; Li, J.; Pan, W. X.; Fu, J. J.; Zhang, A. Q. Evaluation of the binding performance of flavonoids to estrogen receptor alpha by Autodock, Autodock Vina and Surflex-Dock. *Ecotoxicol. Environ. Saf.* **2022**, *233*, 113323.

(25) Bren, U.; Oostenbrink, C. Cytochrome P450 3A4 inhibition by ketoconazole: tackling the problem of ligand cooperativity using molecular dynamics simulations and free-energy calculations. *J. Chem. Inf. Model.* **2012**, *52*, 1573−1582.

(26) Ekroos, M.; Sjögren, T. Structural basis for ligand promiscuity in cytochrome P450 3A4. *Proc. Natl. Acad. Sci. U.S.A.* **2006**, *103*, 13682−13687.

(27) Guengerich, F. P. Cytochrome P450 and chemical toxicology. *Chem. Res. Toxicol.* **2008**, *21*, 70−83.

(28) Hermano Sampaio Dias, A.; Yadav, R.; Mokkawes, T.; Kumar, A.; Skaf, M. S.; Sastri, C. V.; et al. Biotransformation of bisphenol by human cytochrome P450 2C9 enzymes: A density functional theory study. *Inorg. Chem.* **2023**, *62*, 2244−2256.

https://doi.org/10.1021/envhealth.4c00132
Environ. Health 2025, 3, 133−142

(29) Frisch, M. J.; Trucks, G. W.; Schlegel, H. B.; Scuseria, G. E.; Robb, M. A.; Cheeseman, J. R. et al. *Gaussian 16 C.01*; Gaussian, Inc.: 2016.
(30) Louka, S.; Barry, S. M.; Heyes, D. J.; Mubarak, M. Q. E.; Ali, H. S.; Alkhalaf, L. M.; Munro, A. W.; Scrutton, N. S.; Challis, G. L.; de Visser, S. P. Catalytic mechanism of aromatic nitration by cytochrome P450 TxtE: Involvement of a ferric-peroxynitrite intermediate. *J. Am. Chem. Soc.* **2020**, *142*, 15764−15779.
(31) Guidez, E. B.; Gordon, M. S. Dispersion correction derived from First Principles for Density Functional Theory and Hartree−Fock Theory. *J. Phys. Chem. A* **2015**, *119*, 2161−2168.
(32) Riley, K. E.; Vondrášek, J.; Hobza, P. Performance of the DFT-D Method, paired with the PCM implicit solvation model, for the computation of interaction energies of solvated complexes of biological interest. *Phys. Chem. Chem. Phys.* **2007**, *9*, 5555−5560.
(33) Ogliaro, F.; de Visser, S. P.; Cohen, S.; Kaneti, J.; Shaik, S. The experimentally elusive oxidant of cytochrome P450: a theoretical "trapping" defining more closely the "real" species. *Chembiochem* **2001**, *2*, 848−851.
(34) Becke, A. D. Density-functional exchange-energy approximation with correct asymptotic behavior. *Phys. Rev. A* **1988**, *38*, 3098.
(35) Hu, Z.; Ge, H.; Yang, X. Binuclear O_2 activation and hydrogen transfer mechanism for aerobic oxidation of alcohols. *Catal. Sci. Technol.* **2020**, *10*, 2183−2192.
(36) Jensen, K. P.; Roos, B. O.; Ryde, U. Performance of density functionals for first-row transition metal systems. *J. Chem. Phys.* **2007**, *126*, No. 014103.
(37) Vancoillie, S.; Zhao, H.; Radoń, M.; Pierloot, K. Performance of CASPT2 and DFT for relative spin-state energetics of Heme Models. *J. Chem. Theory Comput.* **2010**, *6*, 576−582.
(38) Ji, L.; Ji, S.; Wang, C.; Kepp, K. P. Molecular mechanism of alternative P450-catalyzed metabolism of environmental phenolic endocrine-disrupting chemicals. *Environ. Sci. Technol.* **2018**, *52*, 4422−4431.
(39) Ji, L.; Schüürmann, G. Computational biotransformation profile of paracetamol catalyzed by cytochrome P450. *Chem. Res. Toxicol.* **2015**, *28*, 585−596.
(40) Guo, F.; Chai, L.; Zhang, S.; Yu, H.; Liu, W.; Kepp, K. P.; Ji, L. Computational biotransformation profile of emerging phenolic pollutants by cytochromes P450: phenol-coupling mechanism. *Environ. Sci. Technol.* **2020**, *54*, 2902−2912.
(41) Sakuma, S.; Nakanishi, M.; Morinaga, K.; Fujitake, M.; Wada, S.; Fujimoto, Y. Bisphenol A 3,4-quinone induces the conversion of xanthine dehydrogenase into oxidase in vitro. *Food Chem. Toxicol.* **2010**, *48*, 2217−2222.
(42) Zhao, H. Z.; Wen, J. T.; Xiang, L.; Cai, Z. W. Mass spectrometry investigation of DNA adduct formation from bisphenol A quinone metabolite and MCF-7 cell DNA. *Talanta* **2018**, *182*, 583−589.
(43) Edmonds, J. S.; Nomachi, M.; Terasaki, M.; Morita, M.; Skelton, B. W.; White, A. H. The reaction of bisphenol A 3,4-quinone with DNA. *Biochem. Biophys. Res. Commun.* **2004**, *319*, 556−561.
(44) Lau, S. S.; Monks, T. J.; Everitt, J. I.; Kleymenova, E.; Walker, C. L. Carcinogenicity of a nephrotoxic metabolite of the "non-genotoxic" carcinogen hydroquinone. *Chem. Res. Toxicol.* **2001**, *14*, 25−33.
(45) Ashrap, P.; Zheng, G.; Wan, Y.; Li, T.; Hu, W.; Li, W.; Zhang, W. J.; Zhang, H.; Zhao, Z. B.; Hu, J. Y. Discovery of a widespread metabolic pathway within and among phenolic xenobiotics. *Proc. Natl. Acad. Sci. U.S.A.* **2017**, *114*, 6062−6067.
(46) Liu, L.; Cui, H.; Huang, Y.; Zhou, Y.; Hu, J.; Wan, Y. Enzyme-mediated reactions of phenolic pollutants and endogenous metabolites as an overlooked metabolic disruption pathway. *Environ. Sci. Technol.* **2022**, *56*, 3634−3644.

https://doi.org/10.1021/envhealth.4c00132
Environ. Health 2025, 3, 133−142